Water Reuse

IWA PUBLISHING

Water Reuse Vol 13 No 3, 492 doi: 10.2166/wrd.2023.092

Synthesis and performance of ultrafiltration membranes incorporated with different oxide nanomaterials: experiments and modeling

Nawaf Bin Darwish [a,*], Abdulrahman AlAlawi[a], Hamad AlRomaih[a], Nasser Alotaibi[b] and Musaad AlEid[c]

[a] Desalination Technologies Institute, King Abdulaziz City for Science and Technology (KACST), P. O. Box 6086, Riyadh, Saudi Arabia
[b] Chemistry Department, College of Science, Jouf University, Sakaka, Saudi Arabia
[c] Water Management & Treatment Technologies Institute, King Abdulaziz City for Science and Technology (KACST), P. O. Box 6086, Riyadh, Saudi Arabia
*Corresponding author. E-mail: nbindarwish@kacst.edu.sa

NB, 0000-0002-2228-7546

ABSTRACT

In membrane filtration technology, membrane fouling is the primary obstacle to optimizing efficiency and results in a short membrane lifetime and high operating costs. By incorporating nanomaterials into the membrane synthesis process, a mixed-matrix membrane with significantly enhanced characteristics and performance may be obtained. Graphene oxide (GO), aluminum oxide (Al2O3), tin oxide (SnO2), and titanium oxide (TiO_2) were incorporated into a polyethersulfone (PESU) membrane. The water permeability of the modified membranes showed improvements when compared with the pure membrane. It increased from 65 L/m^2 h bar for the pristine membrane (PES-1) to 143.6, 83.68, 92.12, 75.43 L/m^2 h bar for Al_2O_3 (PES-2), TiO_2 (PES-3), SnO_2 (PES-4), and GO (PES-5) membranes, respectively. It was discovered that the membrane's surface hydrophilicity was significantly and directly affected by the incorporation of nanoparticles. Fouling parameters include R_r (Reversible fouling ratio), R_{ir} (irreversible fouling ratio), R_t (total fouling ratio), and F_{rr} (flux recovery ratio) and were measured to determine the membrane's fouling tendency. The results showed that the membrane's propensity for fouling could be reduced when nanoparticles were incorporated into it. The experimental results are best explained by the cake layer and both standard and intermediate blocking mechanism models, as determined by the traditional single fouling models.

Key words: fouling, models, nanomaterials, ultrafiltration

HIGHLIGHTS

- Ultrafiltration membranes were incorporated with different nanomaterials.
- Different fouling models were fitted to the experimental data.
- The fouling parameters were measured to determine the membrane fouling tendency.
- Water flux improved as a result of pore formation and hydrophilicity enhancement.

1. INTRODUCTION

Ultrafiltration (UF) is a pressurized membrane filtration process for the removal of various macromolecules, colloids, and suspended particles from various solutions and is used in various industrial processes, such as water and wastewater treatments, chemical manufacturing, and food processing. Therefore, membrane contamination, called membrane fouling, is a big problem in UF (Garcia-Ivars *et al.* 2014). Fouling membrane depends on the properties of the membrane surface, including morphology, porosity, and hydrophilicity (Vatanpour *et al.* 2012).

As use of the UF process is growing, efforts to enhance the efficiency of UF-processes become increasingly relevant (Garcia-Ivars *et al.* 2014). Due to their exceptional hydrolytic and thermal stability in addition to strong mechanical properties and chemical stability, sulfone-containing polymers (such as polyethersulfone [PESU] and polysulfones [PSFU]) are commonly used for the preparation of nanofiltration (NF) and UF membranes for water application (AbdulKadir *et al.* 2018). The fouling tendencies of PESU and PSFU in addition to the general polymer membranes are, however, the main concern for real applications as they result in lower fluxes (an increase of the overall energy demand), reduce the life of the membrane, and cause changes in the efficiency of separation (Luque-Alled *et al.* 2020). The intrinsic hydrophobicity of the

membrane material has been identified by several researchers as one of the primary causes of fouling. Industrial wastewater that needs to be treated contains organic foulants with a biological origin, which are generally attracted to hydrophobic membrane surfaces and holes and hence absorb them (Bassyouni *et al.* 2019).

The principal approach to reducing polymeric membrane fouling is to prevent excessive absorption or adhesive processes on the membrane surface since this process prevents or at least slows down colloid build-up (Ng *et al.* 2013). The mixing of polymers and inorganic nanoparticles has recently attracted further attention due to the convenience and mild syntheses required for membrane preparation (Shen *et al.* 2012). It is considered a possible strategy to render higher permeability and antifouling characteristics by incorporating hydrophilic groups into the membrane. The addition of hydrophilic groups to the membrane increases the permeability and antifouling features of the membrane. The incorporation of hydrophilic groups into the membranes usually prevents the deposition of hydrophobic foulants and increases the water permeate flux by creating a surface water layer that facilitates hydrogen bonding with water molecules (Khan *et al.* 2018).

In this study, the influence of the addition of different nanomaterials into the membrane polymer was investigated. Graphene oxide (GO), tin oxide (SnO_2), aluminum oxide (Al_2O_3), and titanium oxide (TiO_2) were used, and their effects on water flux and humic acid fouling-resistance properties were studied.

2. EXPERIMENTAL

2.1. Materials

GO was purchased from MKnano (Canada). Aluminum oxide (Al_2O_3), tin oxide (SnO_2), and titanium oxide (TiO_2) were obtained from Acros Organics (Belgium). PESU (PESU3000, molecular weight 62,000–64,000) from Solvay Advanced Polymers was used to fabricate membrane substrates. PVP (average molecular weight 40,000 Da, Loba Chemie) was used as the additive in the casting solution. Humic acid was obtained from Loba Chemie (India).

2.2. UF process

The experimental setup in this study is illustrated in Figure 1. A cross flow filtration mode was used for all experiments. Pipes, feed tanks, and membrane units were constructed from stainless steel. The permeate was collected in a glass beaker placed on a balance (KERN & SOHN GmbH, China) connected to a laptop to measure the permeate weight over time.

2.3. Membrane preparation

All the membranes were fabricated using a phase inversion technique. Membrane compositions are shown in Table 1. Each membrane's composition was stirred at 70 °C until it formed a homogeneous solution, which was then cooled to room

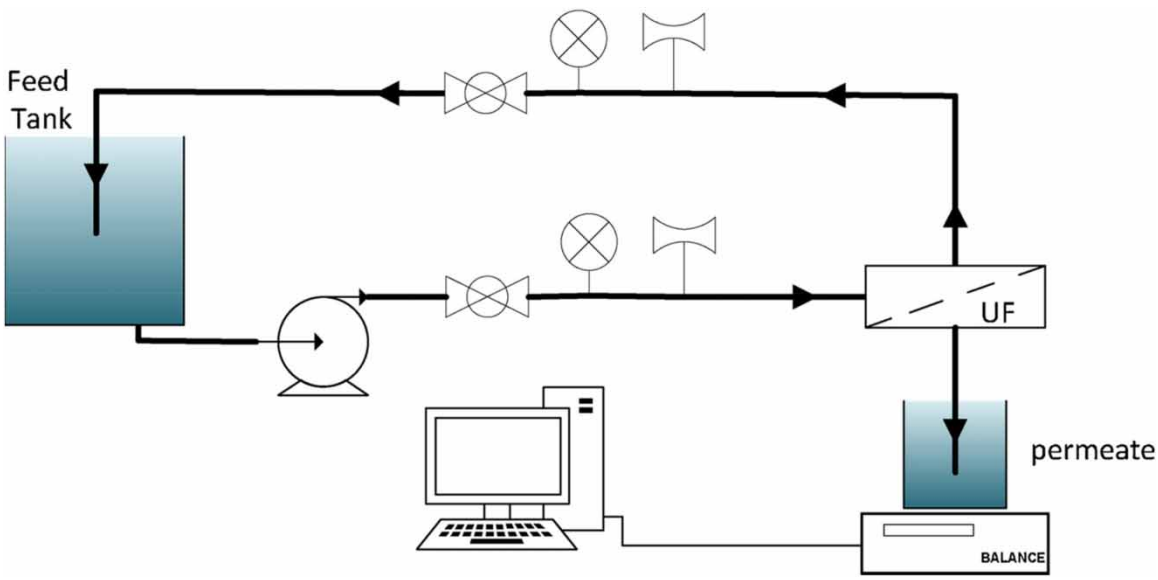

Figure 1 | The experimental setup.

Table 1 | Membranes compositions

Membrane	Polymer (wt %)	polyvinylpyrrolidone (PVP) (wt %)	N-Methylpyrrolidone (NMP) (wt %)	Nanomaterials (wt %)
PES-1	18	6	76	0
PES-2	18	6	75.5	0.5 (Al_2O_3)
PES-3	18	6	75.5	0.5 (TiO_2)
PES-4	18	6	75.5	0.5 (SnO_2)
PES-5	18	6	75.5	0.5 (GO)

PES-1, pristine membrane; PES2–5, modified membranes.

temperature. In an airtight bottle, the dope solution was degassed for 24 h. Using an Elcometer 4340 motorized film applicator with a traverse speed of 70 mm/s, the dope solutions were then cast on a clean glass plate to form a uniform film with a thickness of 150 μm. The film formed on the glass plate was immersed in a 25 °C tap water coagulation bath. The water in the coagulant bath was changed three to four times to remove any excess solvent.

2.4. Membrane characterization

Using the following equations, membrane porosity and mean pore radius were calculated (Mu *et al.* 2019):

Membrane porosity,

$$\varepsilon = \frac{W_w - W_d}{\rho_w \times A \times l} \tag{1}$$

W_w and W_d are the wet and dry membrane weights, respectively, ρ_w is the water density (g/m^3), A is the membrane are (m^2), and l is the membrane thickness (m).

Mean pore radius,

$$r_m = \sqrt{\frac{(2.9 - 1.75\varepsilon) \times 8\eta l Q}{\varepsilon \times A \times \Delta P}} \tag{2}$$

in which η is the water viscosity (8.9×10^{-4} Pa · s), Q is the volume of water permeate per unit time (m^3/s), and ΔP is the operation pressure (0.3 MPa). Each membrane was measured three times, and the average of three measurements was determined to minimize experimental error.

The humic acid rejection ratio (R) was calculated using the following equation:

$$R(\%) = \left(1 - \frac{C_p}{C_f}\right) \times 100 \tag{3}$$

in which C_p and C_f are the humic acid concentration in permeate and feed solutions, respectively.

Water flux was calculated according to the following equation (Kumar *et al.* 2015):

$$J_1 = \frac{V}{A.t} \tag{4}$$

in which V is the volume of water permeate (L), A is the effective membrane area (m^2), and t is the time of permeation (h).

The humic acid solution flux was calculated using the amount of water that permeated the membranes at 5 bar for 2 h. After humic acid solution filtration, the fouled membranes were washed with distilled water for 20 min after which the water flux of cleaned membranes J_2 was measured once more.

The flux recovery ratio (FRR) was estimated as shown in the following equation:

$$F_{rr} = \frac{J_2}{J_1} \times 10 \tag{5}$$

A higher FRR value typically indicates a better UF membrane antifouling performance.

The resistance that develops during the filtration process can be an indication that the membrane is fouled. When a cake/gel layer forms on the membrane's surface, fouling happens as a result of adsorption or because of a build-up of contaminants within the membrane's pores.

The total fouling ratio (R_t) was defined and calculated as shown in the following equation:

$$R_t = (R_r + R_{ir}) \times 100 \tag{6}$$

Reversible fouling ratio (R_r) and irreversible fouling ratio (R_{ir}) were calculated using the equations shown in the following equation (Lin *et al.* 2017):

$$R_r = \frac{J_2 - J_p}{J_1} \times 100 \tag{7}$$

$$R_{ir} = \frac{J_1 - J_2}{J_1} \times 100 \tag{8}$$

Scanning electron microscopy (SEM) images of the membrane's surface and cross-section were captured with a JSM-7100 F instrument (JEOL, USA). Humic acid concentration was measured using Lambda 365 ultraviolet/visible (UV/Vis) Spectrophotometer.

2.5. Modeling for membrane fouling process

Standard, complete, and intermediate blocking methods and cake filtration are examples of traditional models that only consider one mechanism. Figure 2 illustrates the schematic representation of these classical models. Particles enter the pores and cause pore constriction during standard blocking. The surface particle deposit forms during cake filtration. The physical concept of intermediate blocking involves the concurrent occurrence of pore blocking and surface deposit at the same time (Koonani & Amirinejad 2019).

Several mathematical models have been developed to describe the causes of pore blocking and cake layer fouling induced by impurities present during the filtration process (Huang *et al.* 2020). Four traditional single models were proposed by Hermans and Bredée (Hermans 1936). Hermia's models (Hermia 1982) are based on classical constant-pressure dead-end

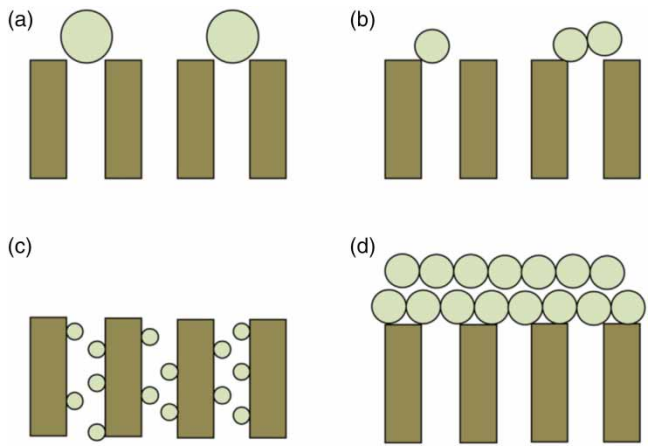

Figure 2 | Schematic drawing of the porous membrane fouling mechanism. (a) Complete blocking, (b) Intermediate blocking, (c) Standard blocking and (d) Cake layer formation (Teow *et al.* 2017).

filtration equations. These equations consider four primary types of membrane fouling and include complete, intermediate, and standard blocking and formation of a cake layer. These models can be modified to consider a crossflow configuration (Corbatón-Báguena *et al.* 2015). Table 2 displays the linear expressions of the four classical single models.

2.5.1. Complete pore blocking

Under the condition of complete pore blocking, it is expected that each particle, upon reaching the surface of the membrane, blocks some membrane pores. This process ensures that no superposition of particles occurs and that the blocked surface area is proportionate to the volume of permeate (Razi *et al.* 2012). Consequently, the effective number of pores decreases during filtration, while the assumed area of each pore remains constant (Sampath *et al.* 2014). An expression for the total volume of filtrate (V) as a function of time (t) is shown in the following equation:

$$V = \frac{J_0}{K_b}(1 - \exp(-K_b\, t)) \tag{9}$$

2.5.2. Standard pore blocking

Standard pore blocking occurs when particles with diameters considerably smaller than those of the membrane pores enter the pores and deposit on the insides of the pore walls, which eventually can cause the pores to become blocked and the pore volume to decrease. According to the following expression, this decline is proportional to time:

$$V = \left(\frac{1}{J_0\, t} + \frac{K_s}{2}\right)^{-1} \tag{10}$$

2.5.3. Intermediate pore blocking

In this situation, every particle that reaches the membrane has the potential to block certain pores or to condense on top of the other particles. As a result, the particles in the membrane are likewise proportional to the volume of permeate that passes through it, but this process is less restrictive than complete pore blocking. The equation that describes the relationship between filtrate volume and time is shown in the following:

$$V = \frac{1}{K_i} \ln(1 + K_i\, J_0\, t) \tag{11}$$

2.5.4. Cake filtration

The cake filtration model was used to explain the situation in which the diameter of the arriving particles is greater than the diameter of the membrane pores. As a result of the cake filtration process, the pores of the membrane are already blocked, and a cake layer forms on the surface of the membrane. This layer thickens with time, which ultimately results in a decrease in

Table 2 | Membrane fouling models for the constant-pressure UF process

Model	Expression	Parameter
Cake layer	$\frac{1}{J^2} = \frac{1}{J_0^2} + k_c t$	k_c (s/m^2)
Complete blocking	$\frac{1}{J} = \frac{1}{J_0} + k_b t$	k_b (s^{-1})
Intermediate blocking	$\frac{1}{\sqrt{J}} = \frac{1}{\sqrt{J_0}} + k_i t$	k_i (m^{-1})
Standard blocking	$\ln(J) = \ln(J_0) - k_s t$	k_s (m^{-1})

flux. As a model, it may be defined as shown in the following equation:

$$V = \frac{1}{K_c J_0}\left(\sqrt{1 + 2K_c J_0^2 t} - 1\right) \tag{12}$$

3. RESULTS AND DISCUSSION

3.1. Membrane characteristics

Membrane porosities and mean pore sizes are summarized in Table 3. The porosity increased from 80.34% for the pure membrane PES-1 to 83.52, 81.61, 83.13, and 81% for the PES-2, -3, -4, and -5 modified membranes, respectively, while the mean pore size increased from 6.25 nm for PES-1 to 8.06, 6.86, 7.58, and 6.42 nm for PES-2, -3, -4, and -5, respectively. The results showed that the addition of nanoparticles enhanced the mean pore size and porosity (Zhu *et al.* 2018). During the phase inversion process, hydrophilic polymeric nanoparticles cause a significant increase in the exchange rate of both the solvent and non-solvent, leading to an increase in the mean pore size and a notable boost in membrane permeability. At the same time, the nanoparticles reorganize favorably on the surface, which leads to an increase in hydrophilicity and thus facilitates an increase in the membranes' antifouling properties.

Water contact angle for the fabricated membranes is shown in Figure 3. The pristine membrane (PES-1) recorded the highest contact angle of 67.4° while the water contact angles of the modified membranes were 48.5, 64.5, 56.4, and 57.1° for PES-2, -3, -4, and -5, respectively. The addition of nanoparticles to the membrane was found to produce a significant and direct impact on the surface hydrophilicity of the membranes (Zhu *et al.* 2018).

The surface and cross-section SEM images of the fabricated membranes are shown in Figures 4 and 5, respectively. Some of the nanomaterial particles were found to have aggregated in the samples. The contrast between the two pictures clearly

Table 3 | Membrane properties

Membrane	Contact angle	Porosity (%)	Mean pore radius (nm)
PES-1	67.4	80.34	6.25
PES-2	48.5	83.52	8.06
PES-3	64.9	81.61	6.86
PES-4	56.4	83.13	7.58
PES-5	57.1	81.00	6.42

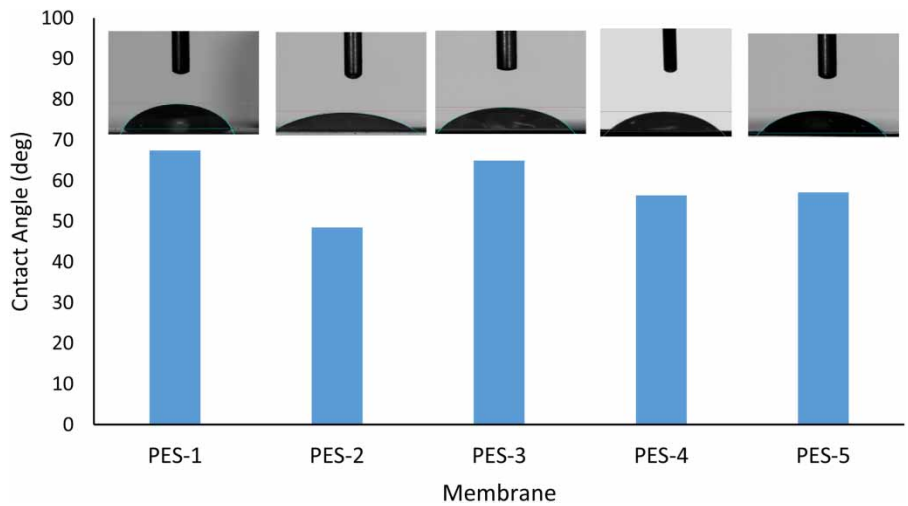

Figure 3 | Water contact angle of the fabricated membranes.

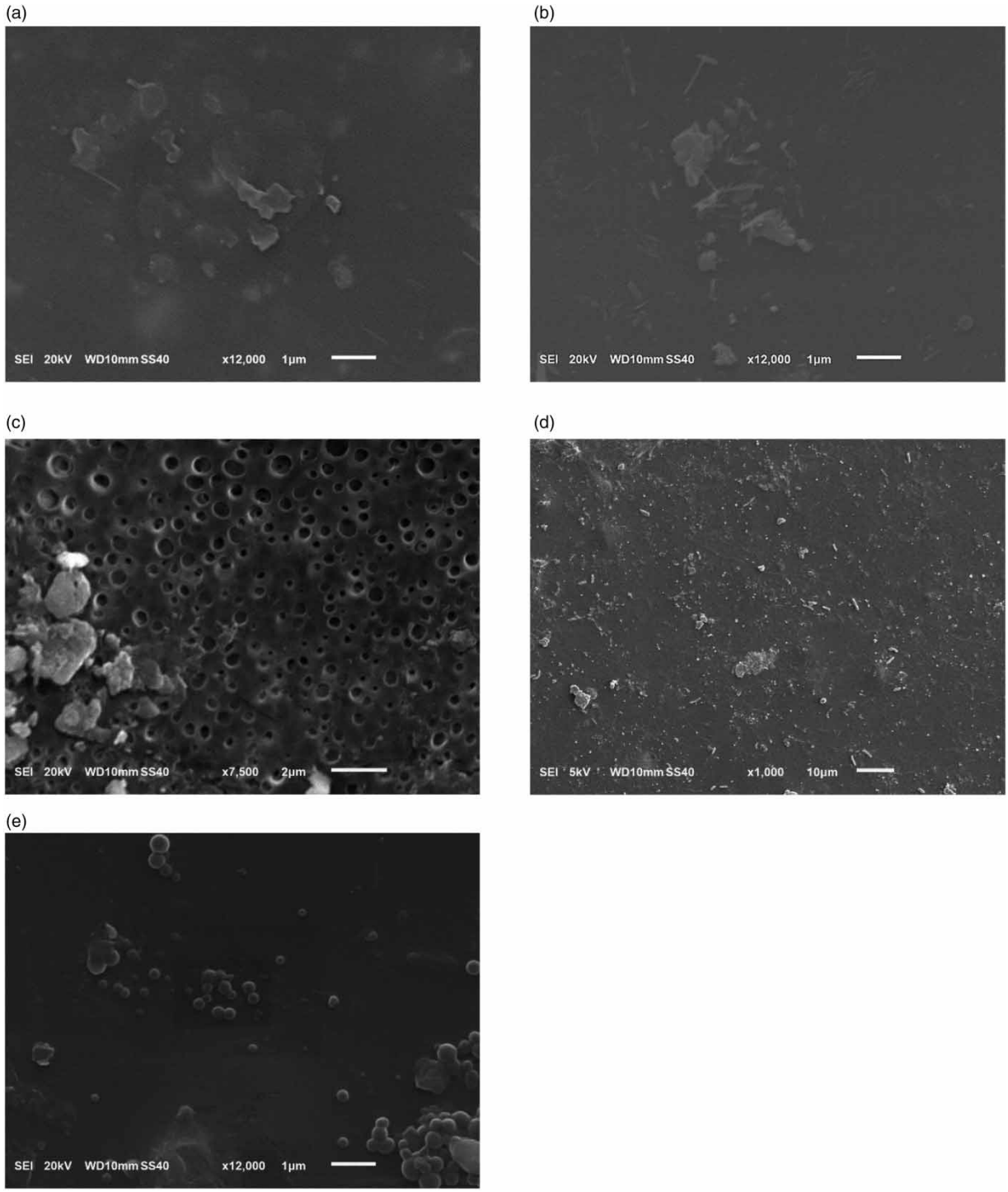

Figure 4 | Surface scanning electron microscopy (SEM) images of the pristine (PES-1)and modified (PES 2–5) membranes (a) PES-1, (b) PES-2, (c) PES-3, (d) PES-4, (e) PES-5.

demonstrates that nanoparticles are there and are most noticeably on the surface. All membranes displayed a typical asymmetric membrane structure as seen in cross-sectional photographs (Figure 5) with a thick outer layer, a porous inner layer, and fully formed macropores at the bottom.

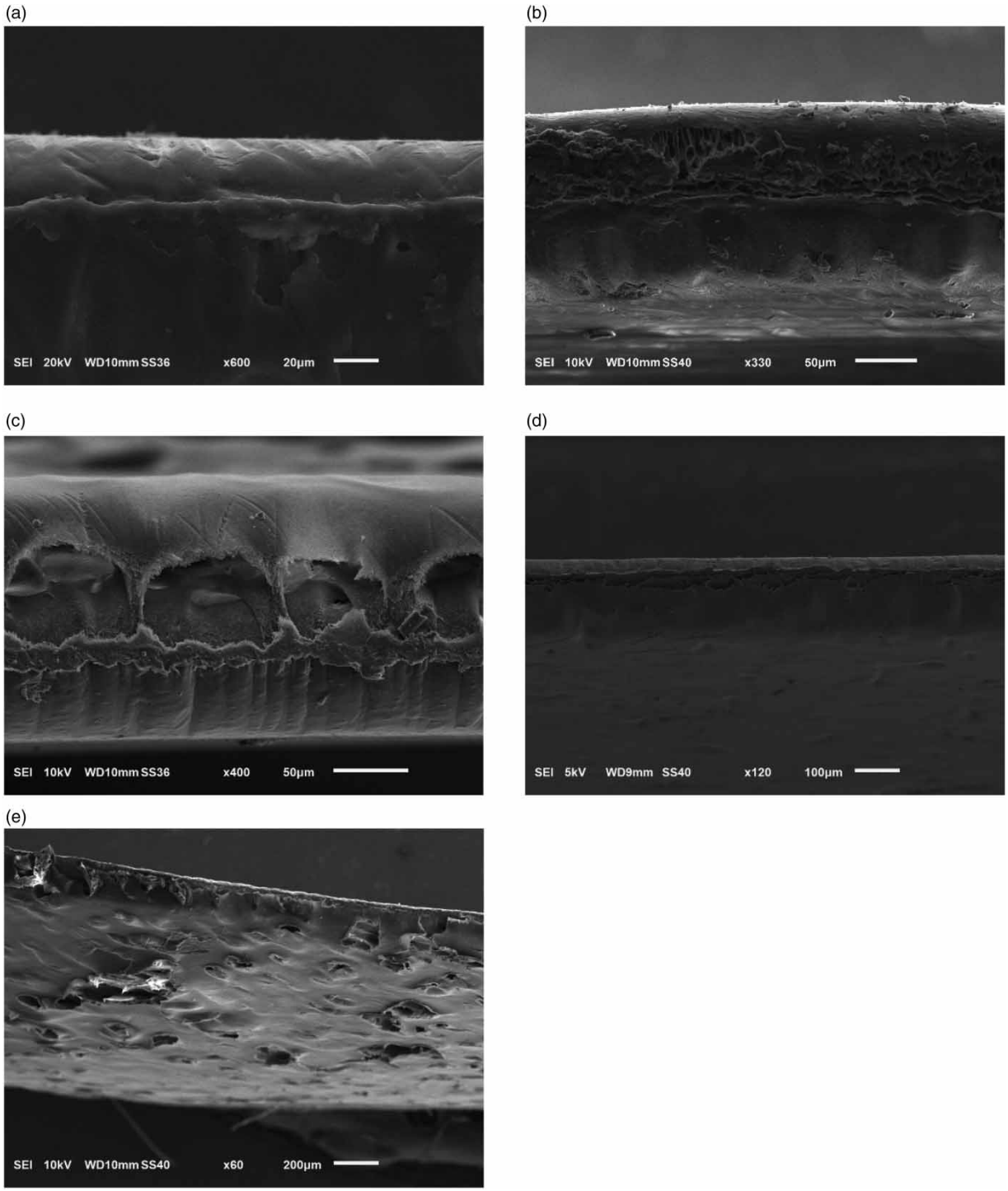

Figure 5 | Cross-section SEM images of the membranes (a) Polyether sulfone (PES)-1, (b) PES-2, (c) PES-3, (d) PES-4, (e) PES-5.

3.2. Pure water flux

As can be observed in Figure 6, all of the modified membranes displayed a higher water permeability than the pure membrane PES-1; specifically, the PES-2 membrane displayed the highest value of 143.6 L/m^2 h bar followed by the PES-4 membrane at 92.12 L/m^2 h bar and 83.68, 75.43 L/m^2 h bar for PES-3, and PES-5 membranes, respectively. In most cases, the pure water flux increases noticeably due to pore formation and hydrophilicity enhancement. This finding agrees with the sequential

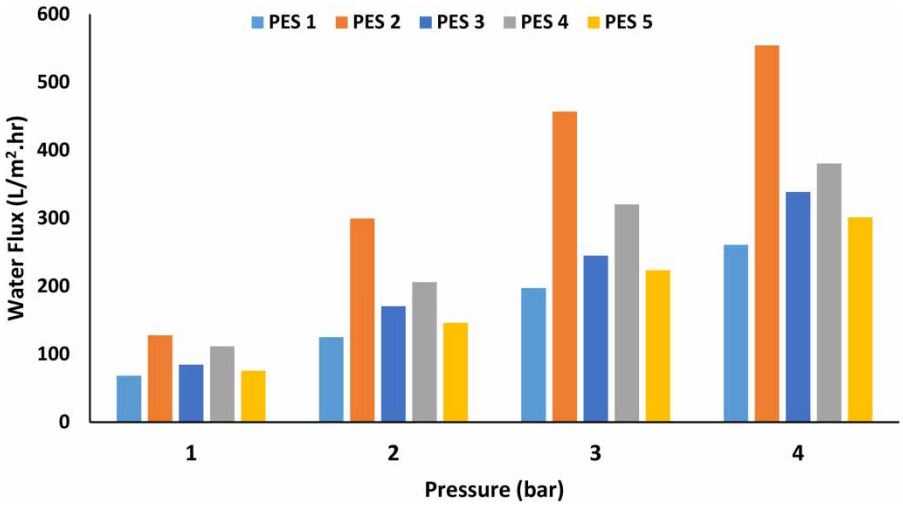

Figure 6 | Pure water flux of the fabricated membranes.

order of contact angle obtained for Al_2O_3–SnO_2–TiO_2–GO modified membranes. Thus, the effect of adding metal–oxide particles on promoting pore formation may be dependent on the particle density close to the membrane surface (María Arsuaga *et al.* 2013; Liu *et al.* 2018; Esfahani *et al.* 2019).

3.3. Analysis of fouling and performance of membranes

Figure 7 shows the flux performance for the humic acid filtration process. These results indicate that the presence of nanoparticles leads to a reduction in the fouling tendency of the membranes.

Fouling parameters, such as R_{ir}, R_r, R_t, and F_{rr}, of membranes were calculated to obtain information about their antifouling properties. A summary of these parameters for non-composite and nanocomposite membranes is shown in Table 4. Since the modified membranes have lower R_t values, this finding indicates that they have higher water flux values and less fouling after UF of the humic acid solution.

Two types of fouling exist: (1) reversible and (2) irreversible. Irreversible fouling is important in membrane filtration performance because the corresponding permeation flux caused by this type of fouling cannot be recovered by cleaning, whereas in the case of reversible fouling, the contaminant is only loosely attached to the surface of the membrane, and it is possible to remove contaminants by washing the membrane with water.

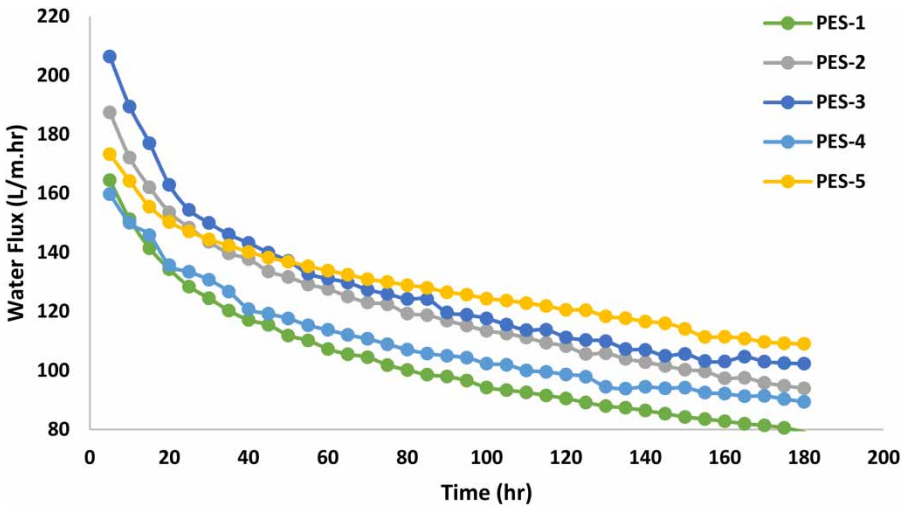

Figure 7 | Fabricated membranes water flux during humic acid filtration.

Table 4 | Fouling parameters of the fabricated membranes

Membrane	R_r	R_{ir}	R_t	F_{rr}
PES-1	10.24	54.11	64.35	45.89
PES-2	23.65	32.87	56.52	65.13
PES-3	25.01	32.5	57.51	67.5
PES-4	30.95	20.57	51.52	79.43
PES-5	28.03	26.23	54.26	73.77

Table 5 | Membrane fouling model results

	Standard blocking		Complete blocking		Intermediate blocking		Cake layer	
Membrane	K_c (s/m^2)	R^2	K_b (s^{-1})	R^2	K_i (m^{-1})	R^2	K_s (m^{-1})	R^2
PES-1	8.3144	0.9562	0.00005	0.9088	0.1987	0.9531	24,628	0.9252
PES-2	6.8844	0.9643	0.00006	0.9185	0.1606	0.9726	22,594	0.9318
PES-3	7.9866	0.9585	0.00006	0.8827	0.162	0.954	22,678	0.9225
PES-4	6.5938	0.9599	0.00006	0.9003	0.155	0.9588	22,988	0.9235
PES-5	7.969	0.951	0.00004	0.9265	0.1005	0.9664	22,110	0.9286

Irreversible fouling (R_{ir}) of the pure PES membrane (PES-1) was found to be 54.11%, while for the nanocomposite membranes, PES-2–5 had irreversible fouling percentages of 32.87, 32.5, 20.57, and 26.23%, respectively. In the reversible fouling case, when compared with the R_r of a pure membrane (10.24%), the R_r values of modified membranes, PES-2 (23.65%), PES-3 (25.01%), PES-4 (30.95%), and PES-5 (28.03%) are all noticeably higher.

Incorporating nanomaterials has been shown to significantly mitigate membrane fouling, even the most intractable forms of irreversible fouling. As can be seen, the improved antifouling performance can be attributed to the increased hydrophilicity of the membrane on its surface in addition to the surface pore size and cross-sectional structures that are preferable (Xu *et al.* 2017; Liu *et al.* 2018).

It is commonly known that a higher flux recovery ratio (F_{rr}) value indicates greater membrane-associated fouling resistance. As compared to other membranes, PES-1 has a lower FRR of 45.89%. Due to its highly hydrophilic and smooth surface contact with the humic acid solution, PES-4 had the highest FRR of any of the other fabricated membranes (79.4%).

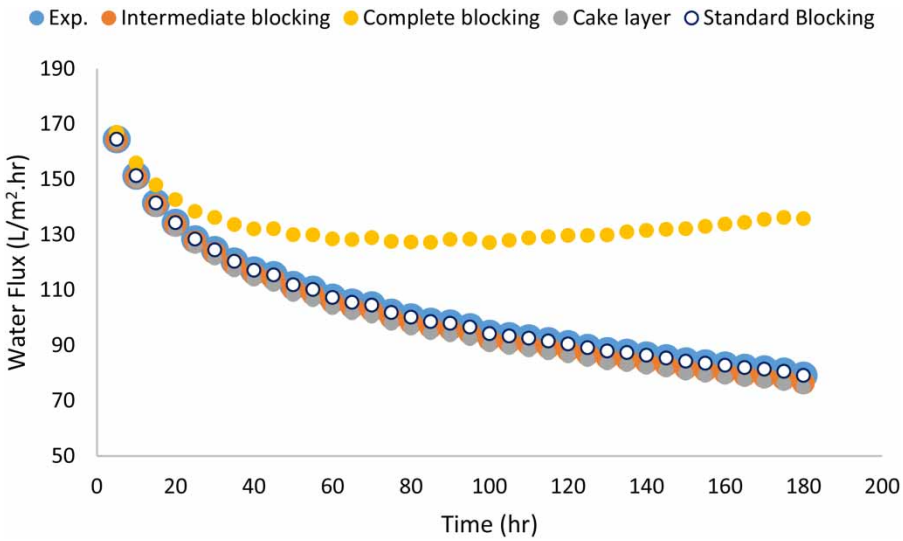

Figure 8 | Experimental permeate flux and single fouling models for PES-1 membrane.

3.4. Modeling of filtration process

Table 5 displays the values of the fit parameters (k-values) in addition to the coefficient of determination (R^2) for membranes.

Two single models (cake layer and standard or intermediate blocking) showed good linear fitting ($R^2 > 0.95$) compared to the other two models (cake layer and complete blocking). This finding suggests that many different fouling mechanisms were taking place at the same time when viewed from a statistical point of view.

Membrane fouling intensity may be studied using the physical principle of Hermia's fitted parameters (k-values), namely, those membranes with higher k-values are more likely to become fouled (Heidari *et al.* 2019). In Table 4, a comparison of Hermia's fitted parameters reveals that PES-1 (pure membrane) has the lowest value. This finding indicates that the membrane's propensity for fouling is reduced when nanoparticles have been incorporated into it.

The flux decline during filtration is illustrated in Figures 8–12 using data from experiments and single fouling models. The figures clearly illustrate that the cake layer and standard and intermediate blocking models best explain the experimental results.

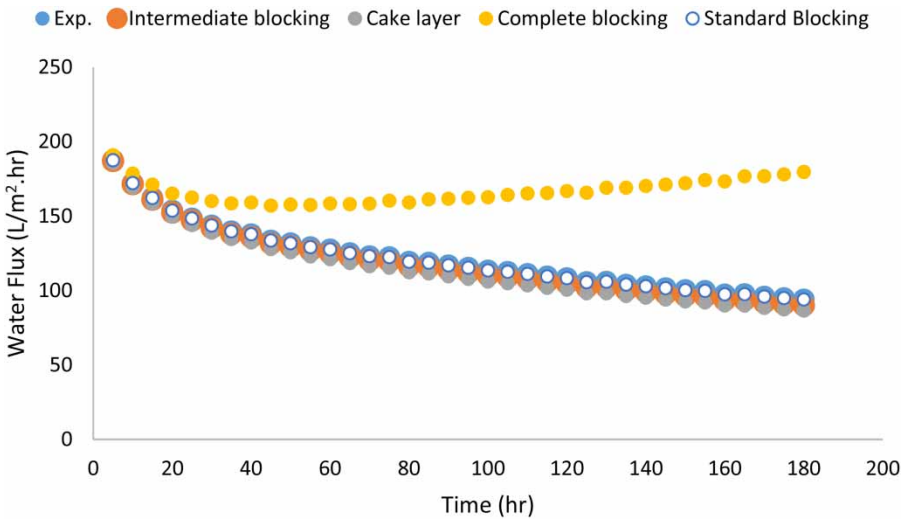

Figure 9 | Experimental permeate flux and single fouling models for PES-2 membrane.

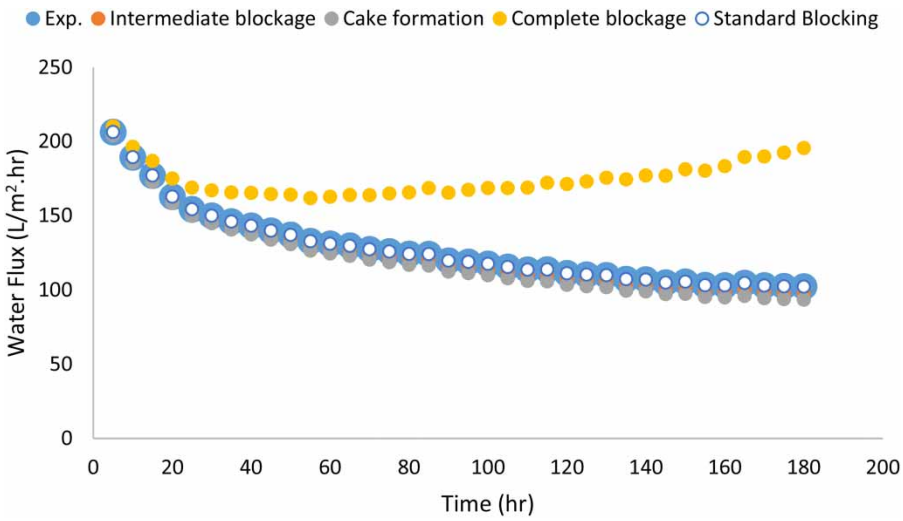

Figure 10 | Experimental permeate flux and single fouling models for PES-3 membrane.

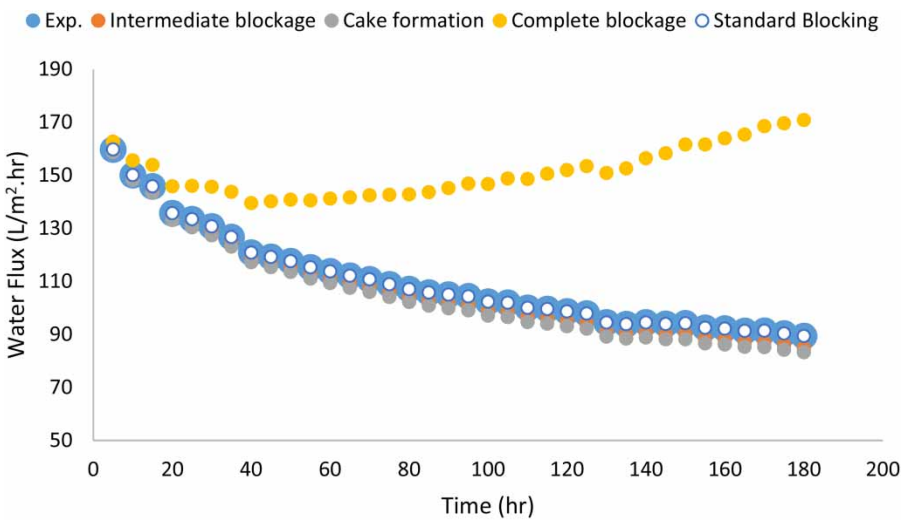

Figure 11 | Experimental permeate flux and single fouling models for PES-4 membrane.

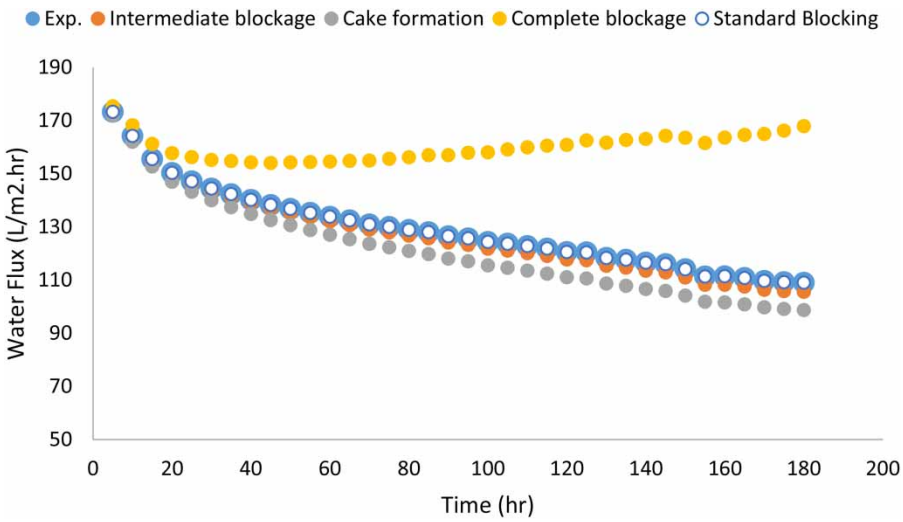

Figure 12 | Experimental permeate flux and single fouling models for PES-5 membrane.

4. CONCLUSION

The incorporation of nanomaterial particles into a membrane substrate can produce an improvement in membrane performance. GO, aluminum oxide (Al_2O_3) tin oxide (SnO_2), and titanium oxide (TiO_2) were used in this study and incorporated into PESU. The water flux of the modified membranes improved when compared with the membrane without a nanomaterial. Increases were seen in PES-2 (Al_2O_3), PES-3 (TiO_2), PES-4 (SnO_2), and PES-5 (GO) from 65 L/m^2 h bar for the pristine membrane (PES-1) to 143.6, 83.68, 92.12, and 75.43 L/m^2 h bar, respectively. The integration of nanoparticles was found to have a major and direct impact on the hydrophilicity of the membrane's surface.

The fouling parameters, including R_r, R_{ir}, R_t, and F_{rr} were applied to determine the fouling tendency of the membranes. The results showed that membrane propensity for fouling is reduced when nanoparticles have been incorporated into it.

The results show that the cake layer and standard and intermediate blocking mechanism models best explain the experimental results.

DATA AVAILABILITY STATEMENT

All relevant data are included in the paper or its Supplementary Information.

CONFLICT OF INTEREST

The authors declare there is no conflict.

REFERENCES

AbdulKadir, C. W., Yunos, K. F. M., Hassan, A. R. & Amin, N. A. M. 2018 Fabrication and performance of PSf/CA blend ultrafiltration membrane on effect of different of polymer ratio. *Journal of Advanced Research in Materials Science* **45**, 1–14.

Bassyouni, A. M., Abdel-Aziz, M. H., Zoromba, M. S., Abdel-Hamid, S. M. S. & Drioli, E. 2019 A review of polymeric nanocomposite membranes for water purification. *Journal of Industrial and Engineering Chemistry* **73**, 19–46.

Corbatón-Báguena, M.-J., Álvarez-Blanco, S. & Vincent-Vela, M.-C. 2015 Fouling mechanisms of ultrafiltration membranes fouled with whey model solutions. *Desalination* **360**, 87–96.

Esfahani, M. R., Aktij, S. A., Dabaghian, Z., Firouzjaei, M. D., Rahimpour, A., Eke, J., Escobar, I. C., Abolhassani, M., Greenlee, L. F., Esfahani, A. R., Sadmani, A. & Koutahzadeh, N. 2019 Nanocomposite membranes for water separation and purification: fabrication, modification, and applications. *Separation and Purification Technology* **213**, 465–499.

Garcia-Ivars, A. J., Alcaina-Miranda, M.-I., Iborra-Clar, M.-I., Mendoza-Roca, J.-A. & Pastor-Alcañiz, L. 2014 Enhancement in hydrophilicity of different polymer phase-inversion ultrafiltration membranes by introducing PEG/Al_2O_3 nanoparticles. *Separation and Purification Technology* **128**, 45–57.

Heidari, S., Amirinejad, M. & Jahangirian, H. 2019 Investigation of fouling mechanisms using surface morphology and physicochemical membrane features. *Chemical Engineering & Technology* **42**, 1310–1320.

Hermans, P. 1936 Principles of the mathematical treatment of constant-pressure filtration. *Journal of the Society of Chemical Industry* **55**, 1.

Hermia, J. 1982 Constant pressure blocking filtration laws: application to power-law non-Newtonian fluids. *Institution of Chemical Engineers* **60**, 183–187.

Huang, B., Gu, H., Xiao, K., Qu, F., Yu, H. & Wei, C. 2020 Fouling mechanisms analysis via combined fouling models for surface water ultrafiltration process. *Membranes* **10**, 149.

Khan, A., Sherazi, T. A., Khan, Y., Li, S., Naqvi, S. A. R. & Cui, Z. 2018 Fabrication and characterization of polysulfone/modified nanocarbon black composite antifouling ultrafiltration membranes. *Journal of Membrane Science* **554**, 71–82.

Koonani, H. & Amirinejad, M. 2019 Combined three mechanisms models for membrane fouling during microfiltration. *Journal of Membrane Science and Research* **5**, 274–282.

Kumar, M., McGlade, D., Ulbricht, M. & Lawler, J. 2015 Quaternized polysulfone and graphene oxide nanosheet derived low fouling novel positively charged hybrid ultrafiltration membranes for protein separation. *RSC Advances* **5**, 51208–51219.

Lin, Y., Loh, C. H., Shi, L., Fan, Y. & Wang, R. 2017 Preparation of high-performance Al_2O_3/PES composite hollow fiber UF membranes via facile in-situ vapor induced hydrolyzation. *Journal of Membrane Science* **539**, 65–75.

Liu, Q., Huang, S., Zhang, Y. & Zhao, S. 2018 Comparing the antifouling effects of activated carbon and TiO_2 in ultrafiltration membrane development. *Journal of Colloid and Interface Science* **515**, 109–118.

Luque-Alled, J. M., Abdel-Karim, A., Alberto, M., Leaper, S., Perez-Page, M., Huang, K., Vijayaraghavan, A., El-Kalliny, A. S., Holmes, S. M. & Gorgojo, P. 2020 Polyethersulfone membranes: from ultrafiltration to nanofiltration via the incorporation of APTS functionalized-graphene oxide. *Separation and Purification Technology* **230**, 115836.

María Arsuaga, J., Sotto, A., del Rosario, G., Martínez, A., Molina, S., Teli, S. B. & de Abajo, J. 2013 Influence of the type, size, and distribution of metal oxide particles on the properties of nanocomposite ultrafiltration membranes. *Journal of Membrane Science* **428**, 131–141.

Mu, Y., Zhu, K., Luan, J., Zhang, S., Zhang, C., Na, R., Yang, Y., Zhang, X. & Wang, G. 2019 Fabrication of hybrid ultrafiltration membranes with improved water separation properties by incorporating environmentally friendly taurine modified hydroxyapatite nanotubes. *Journal of Membrane Science* **577**, 274–284.

Ng, L. Y., Mohammad, A. W., Leo, C. P. & Hilal, N. 2013 Polymeric membranes incorporated with metal/metal oxide nanoparticles: a comprehensive review. *Desalination* **308**, 15–33.

Razi, B., Aroujalian, A. & Fathizadeh, M. 2012 Modeling of fouling layer deposition in cross-flow microfiltration during tomato juice clarification. *Food and Bioproducts Processing* **90**, 841–848.

Sampath, M., Shukla, A. & Rathore, A. S. 2014 Modeling of filtration processes – microfiltration and depth filtration for harvest of a therapeutic protein expressed in *Pichia pastoris* at constant pressure. *Bioengineering* **1**, 260–277.

Shen, L., Bian, X., Lu, X., Shi, L., Liu, Z., Chen, L., Hou, Z. & Fan, K. 2012 Preparation and characterization of ZnO/polyethersulfone (PES) hybrid membranes. *Desalination* **293**, 21–29.

Teow, Y. H., Ooi, B. S. & Ahmad, A. L. 2017 Fouling behaviours of PVDF-TiO_2 mixed-matrix membrane applied to humic acid treatment. *Journal of Water Process Engineering* **15**, 89–98.

Vatanpour, B. V., Madaeni, S. S., Moradian, R., Zinadini, S. & Astinchap, B. 2012 Novel antibifouling nanofiltration polyethersulfone membrane fabricated from embedding TiO_2 coated multiwalled carbon nanotubes. *Separation and Purification Technology* **90**, 69–82.

Xu, H., Ding, M., Liu, S., Li, Y., Shen, Z. & Wang, K. 2017 Preparation and characterization of novel polysulphone hybrid ultrafiltration membranes blended with N-doped GO/TiO_2 nanocomposites. *Polymer* **117**, 198–207.

Zhu, K., Mu, Y., Zhang, M., Liu, Y., Na, R., Xu, W. & Wang, G. 2018 Mixed matrix membranes decorated with in situ self-assembled polymeric nanoparticles driven by electrostatic interaction. *Journal of Materials Chemistry A* **6**, 7859–7870.

First received 4 July 2023; accepted in revised form 23 August 2023. Available online 1 September 2023